

Electronic Supplementary Information

AI-assisted mass spectrometry imaging with *in-situ* image segmentation for subcellular metabolomics analysis

Cong-Lin Zhao,^{†a} Han-Zhang Mou,^{†a} Jian-Bin Pan,^{†a} Lei Xing,^{*a} Yuxiang Mo,^b Bin Kang,^{*a} Hong-Yuan Chen,^a and Jing-Juan Xu^{*a}

[a] C. L. Zhao, H. Z. Mou, J. B. Pan, L. Xing, Prof. B. Kang, Prof. H. Y. Chen, Prof. Dr. J. J. Xu
State Key Laboratory of Analytical Chemistry for Life Science, School of Chemistry and Chemical
Engineering, Nanjing University, Nanjing 210023 (China)

E-mail: xl1992@nju.edu.cn

binkang@nju.edu.cn

xujj@nju.edu.cn

[b] Prof. Dr. Y. X. Mo

State Key Laboratory of Low-Dimensional Quantum Physics, Department of Physics, Tsinghua
University, Beijing 100084 (China)

Table of Contents

| | |
|---|----|
| 1. Experimental Section | 3 |
| 1.1 Chemicals | 3 |
| 1.2 Cell Culture | 3 |
| 1.3 Cell Fixation and Lyophilization | 3 |
| 1.4 Fluorescence Measurement | 3 |
| 1.5 MS Imaging, Data Processing and Statistical Analysis..... | 4 |
| 2. Figures and Tables | 5 |
| 3. References | 11 |

1. Experimental Section

1.1 Chemicals

1 × PBS buffer and high sugar dulbecco's modified eagles medium (DMEM) were purchased from Jiangsu Keygen Biotechnology Co., Ltd. (Nanjing, China). 3-hydroxybutyric acid (3-HBA), doxorubicin (DOX) and epirubicin hydrochloride (EPI·HCl) (> 98% purity) were purchased from Shanghai Yuanye Biotechnology Co., Ltd. (Shanghai, China). The amino acid (glutamate and aspartate) (98% purity) and 4% paraformaldehyde (4% PFA) fix solution were purchased from Sangon Biotech (Shanghai) Co., Ltd. Choline (40% aqueous solution) and sinapic acid (98% purity) were purchased from Tianjin Xisisi Opude Technology Co., Ltd. (Tianjin, China). L-dope (≥ 99% purity) was purchased from Shanghai Dibo Biotechnology Co., Ltd. (Shanghai, China). The sterilized water was purchased from Shanghai Jierui Bioengineering Co., Ltd. (Shanghai, China).

1.2 Cell Culture

HeLa cells were purchased from the American Model Culture Repository (ATCC). The ratio of Australian fetal bovine (FBS) to DMEM high-sugar medium in the culture medium used for Hela cells was 1:9. Cells were cultured in an incubator at 37 °C and 5% CO₂. Quartz sheets (15 × 3 × 0.1 mm³) were sonicated with absolute ethanol, transferred quartz sheets to a 35 mm Petri dish on an ultraclean stage, and washed three times (2 mL × 3) with 1 × PBS buffer. Hela cells with a density of approximately 5 × 10⁴/mL were seeded into dishes. After being cultured in an incubator for 24 h, they were washed 3 times with 1 × PBS for subsequent administration.

1.3 Cell Fixation and Lyophilization

DMEM culture medium was used to configure DOX and EPI solutions at a final concentration of 100 μM. The cells were respectively incubated for 3 hours with the above three drugs in an incubator and then washed with 1 × PBS buffer at least 3 times. Then add 4% PFA and fix it in the ultra-clean table for 20 min. This is followed by 3 washes with PBS (2 mL × 3) and 3 times with sterile water (2 mL × 3). Finally, the quartz flakes were transferred to small lyophilized bottles and freeze-dried with a freeze dryer (Labconco Freezone CentriVap, USA) for 24 h. Keep tightly sealed in the freezer compartment of the refrigerator for subsequent cell assay analysis.

1.4 Fluorescence Measurement

Fluorescence images of cells are taken by laser scanning confocal microscopy (ZEISS LSM 710). The cells were cultured with 4', 6-diamido-2-phenylindole (DAPI)

staining solution (Beyotime). The emission ranges of 415-530 nm were collected through the blue channel, using excitation wavelengths of 405 nm. Fluorescence images were captured in 2048×2048 pixels and were acquired using a $40 \times$ lens.

1.5 MS Imaging, Data Processing and Statistical Analysis

The mass spectrometry imaging device was homemade according to the literature.¹ The desorption/ionization source is a VUV laser (~ 130 nm) produced by a mixture of four waves. The laser irradiates vertically to ionize and desorb the sample surface. Then, the m/z signals were eventually collected and amplified by the three microchannel plates (MCP). The entire process was carried out in a high vacuum ($< 5 \times 10^{-5}$ pa) environment. Reflectron TOF-MS operates in positive ion mode. All raw data was preprocessed using Matlab software with a self-written program (MathWorks, Inc., USA), which enables peak alignment, data correction and normalization. Cell segmentation was performed by a self-written program in Matlab software. Mass spectral peaks with signal-to-noise ratio greater than 3 were extracted and peak intensity was normalized. Organize m/z values and normalization strength to form an alignment matrix for machine learning. Utilizing the principal component analysis (PCA) or AI-assisted data analysis to extract the significant information, we measured 10-20 single-cell samples to increase the accuracy of statistical results. At least three independent MSI measurements for different biological samples were performed in the above experiments to ensure the repeatability of the experiment and very similar results were achieved. Execute different machine learning models in OmicShare Tools (<https://www.omicshare.com/tools/Home/Soft/getsoft>). PCA was used to evaluate the overall trend of within-group aggregation and inter-group separation, and Orthogonal Partial Least Squares-Discriminant Analysis (OPLS-DA) was used to screen for m/z signals that were helpful for the classification of experimental samples. Afterward, all metabolic markers were tentatively annotated and identified based on m/z signals using online databases such as the Human Metabolome Database (HMDB) (<http://www.hmdb.ca/>) and Kyoto Encyclopedia of Genes and Genomes (KEGG) (<https://www.genome.jp/kegg/>). To further understand the metabolic differences, MetaboAnalyst 5.0 (<https://www.metaboanalyst.ca/>) and KEGG databases were carried out to analyze the relevant pathways of the metabolites.

2. Figures and Tables

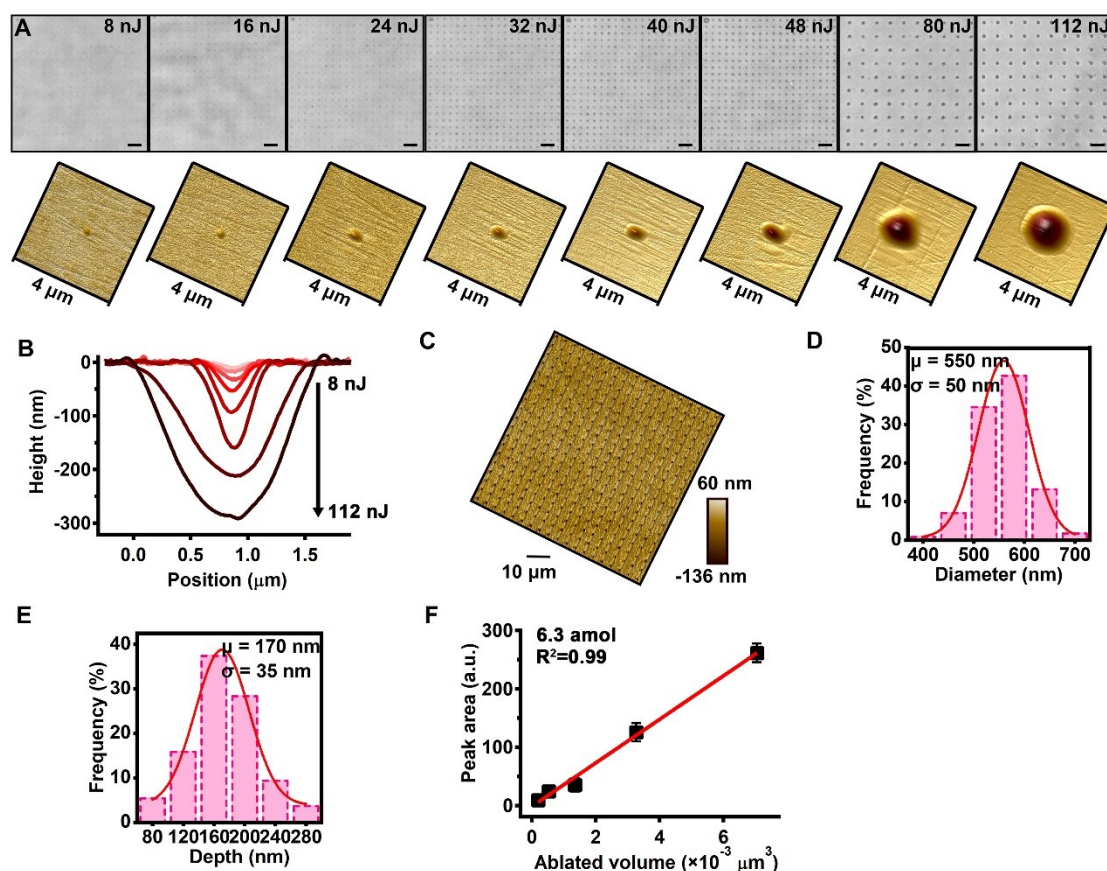


Figure S1. Optical images ($40 \times 40 \mu\text{m}^2$) of ablated crater arrays (1 pulse for each crater) with a 2 or $4 \mu\text{m}$ step size on the surface of polymethyl methacrylate (top row) and atomic force microscope (AFM) images of a single sampling crater (bottom row). The craters were generated by the VUV laser with different intensities from 8 nJ to 112 nJ. Scale bar: $4 \mu\text{m}$. (B) The depth curves of craters showed in (A). (C) AFM image of craters generated by a 48 nJ VUV laser. The diameter (D) and depth (E) histograms of ~ 360 craters in (C). (F) Evaluation of the absolute limit of detection (ALOD) of this AI-SMSI method calculated based on DOX.

The performance of the MSI instrument was evaluated based on a previous device, called vacuum ultraviolet laser desorption/ionization reflection time-of-flight mass spectrometry (VUVDI-RTOF-MS).² The multi-scaled imaging capability of this MSI instrument was verified by ablating the surface of a polymethyl methacrylate, ranging from $\sim 2 \mu\text{m}$ to $\sim 300 \text{ nm}$ (Figure S1A). Meantime, the depth curves corresponding to the craters at different energies showed an almost smooth baseline, even using high laser energy (Figure S1B), which indicated that there was little accumulation of ionic garbage around the crater caused by the thermal effect. Therefore, signal interference will hardly occur between each measuring point. After statistical analysis from ~ 360 ablation craters (Figure S1C), the 48 nJ intensity of the VUV laser with $\sim 550 \text{ nm}$ of diameter (Figure S1D) and $\sim 170 \text{ nm}$ of depth (Figure S1E) was chosen as the desorption/ionization source. Additionally, the absolute limit of detection of this method for DOX was calculated to be $\sim 6.3 \text{ amol}$ (Figure S1F). Accordingly, the step size of 500 nm per pixel was determined to scan and map the single cells.

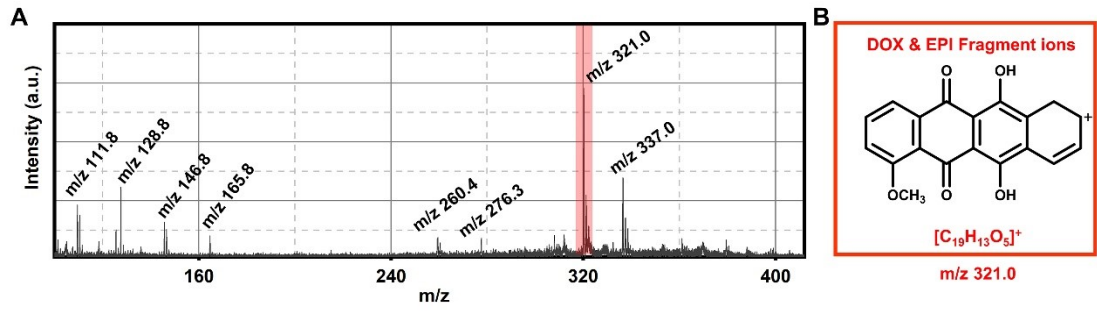


Figure S2. (A) Typical mass spectrum of DOX. (B) Chemical structure of DOX & EPI fragment ions ($[C_{19}H_{13}O_5]^+$, m/z 321.0).

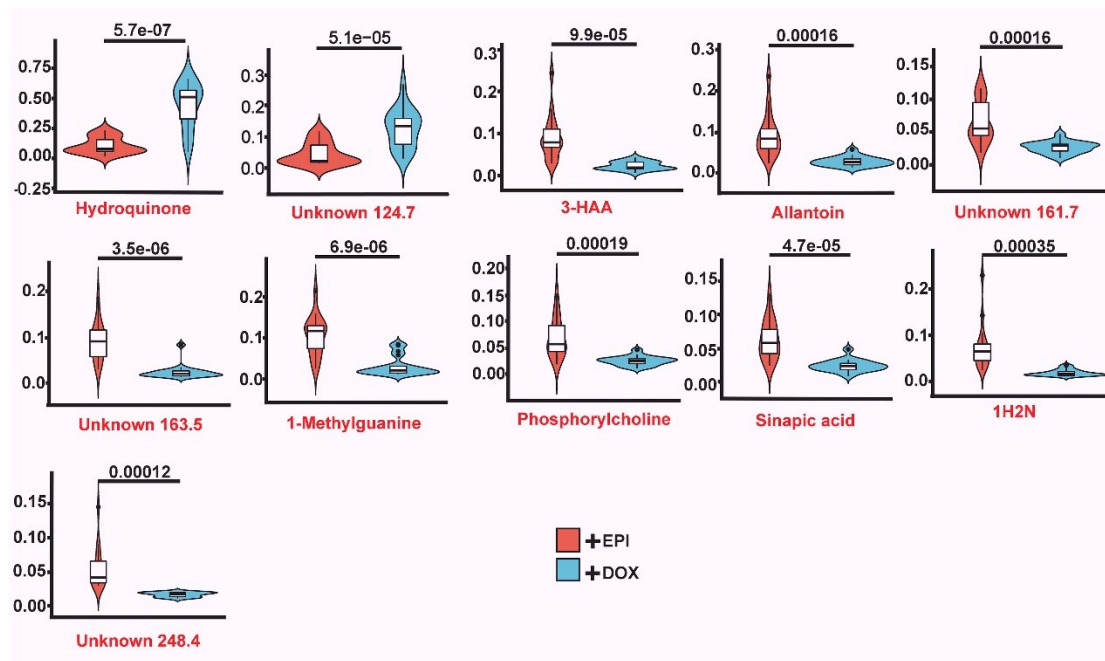


Figure S3. Violin boxes of part metabolites from EPI-treated (red) and DOX-treated (blue) cells with the degree of differentiation.

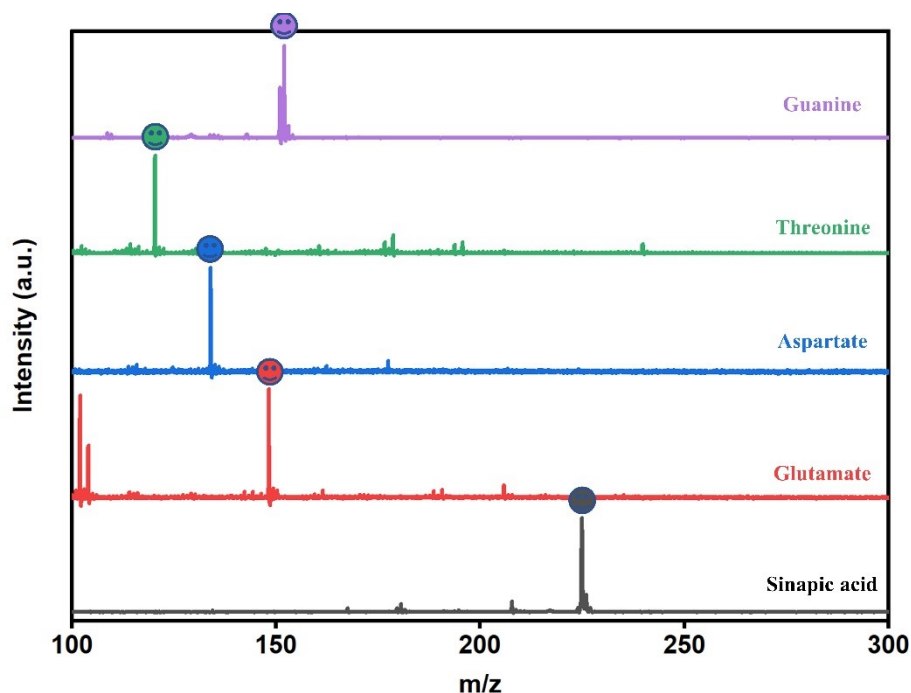


Figure S4. Mass spectra of sinapic acid ($[\text{C}_{11}\text{H}_{12}\text{O}_5+\text{H}]^+$ at m/z 225.1, black line), glutamate ($[\text{C}_5\text{H}_9\text{NO}_4+\text{H}]^+$ at m/z 148.2, red line), spartate ($[\text{C}_4\text{H}_7\text{NO}_4+\text{H}]^+$ at m/z 134.1, blue line), threonine ($[\text{C}_4\text{H}_9\text{NO}_3+\text{H}]^+$ at m/z 120.2, green line), and guanine ($[\text{C}_5\text{H}_5\text{N}_5\text{O}+\text{H}]^+$ at m/z 152.1, purple line).

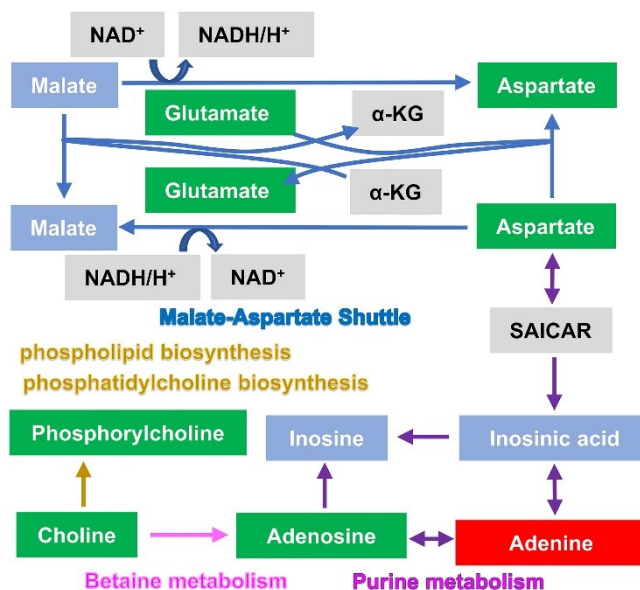


Figure S5. The relational network of key metabolic pathways. Compared to EPI, the upregulated metabolites induced by DOX were displayed on a red background; Downregulated metabolites were shown on a green background; Expressions of metabolites with no significant changes were shown on a blue background; A grey background indicated that it was undetected.

Figure S5 illustrates the relational network of five metabolic pathways with top contributions in the cytoplasm. These pathways include the malate-aspartate shuttle (MAS), purine metabolism, phosphatidylcholine biosynthesis, betaine metabolism, and phospholipid biosynthesis. The MAS is the primary mechanism for transferring

reducing equivalents (NAD, NADH) from the cytosol into mitochondria.³ In mitochondria, these reducing equivalents are utilized in oxidative phosphorylation. This shuttle plays a fundamental role in the energy production process. Purine metabolites not only serve as building blocks for DNA and RNA but also play a significant role in supplying cells with the required energy and cofactors, promoting cell survival and proliferation.⁴⁻⁶ Phospholipid and phosphatidylcholine biosynthesis can regulate lipid metabolism, including lipoproteins, and overall energy metabolism.^{7, 8} Their abnormal expression levels have been linked to disease progression and can influence energy metabolism. Betaine metabolism participates in many important biochemical pathways, such as the biosynthesis of compounds like phosphorylcholine and adenosine, etc.⁹⁻¹¹ As discussed in the main text, these pivotal metabolic pathways are intricately interconnected, influencing the entire metabolic network and providing feedback on the drug-cell interactions and their toxic side effects.

Table S1. Summary of basic information about differential m/z signals between EPI-cultured and DOX-cultured Hela cells.

| Peak No. | Peak (m/z) | Tentative assignment | AUC | Molecular formula | + EPI vs. +DOX | Reference |
|----------|------------|----------------------|-------|---|----------------|-----------|
| 1 | 104.0 | Choline | 0.974 | [C ₅ H ₁₄ NO] ⁺ | Up | 12, 13 |
| 2 | 105.2 | 3-HBA | 0.944 | [C ₄ H ₈ O ₃ +H] ⁺ | Down | 14 |
| 3 | 110.2 | Hydroquinone | 0.926 | [C ₆ H ₆ O ₂] ⁺ | Down | 15 |
| 4 | 120.2 | Threonine | 0.867 | [C ₄ H ₉ NO ₃ +H] ⁺ | Down | Figure S4 |
| 5 | 124.7 | to be verified | 0.883 | - | Down | - |
| 6 | 126.0 | 5-Methylcytosine | 0.978 | [C ₅ H ₇ N ₃ O+H] ⁺ | Up | 16 |
| 7 | 134.1 | Aspartate | 0.975 | [C ₄ H ₇ NO ₄ +H] ⁺ | Up | Figure S4 |
| 8 | 136.1 | Adenine | 0.886 | [C ₅ H ₅ N ₅ +H] ⁺ | Down | 17 |
| 9 | 148.2 | Glutamate | 0.898 | [C ₅ H ₉ NO ₄ +H] ⁺ | Up | Figure S4 |
| 10 | 154.0 | 3-HAA | 0.904 | [C ₇ H ₇ NO ₃ +H] ⁺ | Up | 18, 19 |
| 11 | 159.2 | Allantoin | 0.944 | [C ₄ H ₆ N ₄ O ₃ +H] ⁺ | Up | 20 |
| 12 | 161.7 | to be verified | 0.914 | - | Up | - |
| 13 | 163.5 | to be verified | 0.969 | - | Up | - |
| 14 | 165.0 | 1-Methylguanine | 0.935 | [C ₆ H ₇ N ₅ O] ⁺ | Up | 21 |
| 15 | 184.1 | Phosphorylcholine | 0.917 | [C ₅ H ₁₅ NO ₄ P] ⁺ | Up | 1, 2, 22 |
| 16 | 188.0 | 1H2N | 0.977 | [C ₁₁ H ₈ O ₃] ⁺ | Up | 23 |
| 17 | 225.1 | Sinapic acid | 0.889 | [C ₁₁ H ₁₂ O ₅ +H] ⁺ | Up | Figure S4 |
| 18 | 248.4 | to be verified | 1.000 | - | Up | - |
| 19 | 268.1 | Adenosine | 0.972 | [C ₁₀ H ₁₃ N ₅ O ₄ +H] ⁺ | Up | 20, 24 |

3. References

1. J. Wang, Z. Y. Wang, F. Liu, L. Cai, J. B. Pan, Z. P. Li, S. C. Zhang, H. Y. Chen, X. R. Zhang and Y. X. Mo, *Anal. Chem.*, 2018, **90**, 10009-10015.
2. H. Z. Mou, J. B. Pan, C. L. Zhao, L. Xing, Y. X. Mo, B. Kang, H. Y. Chen and J. J. Xu, *ACS Nano*, 2023, **17**, 10535-10545..
3. K. F. Lanoue and J. R. Williamson, *Metab.Clin. Exp.*, 1971, **20**, 119.
4. A. M. Pedley and S. J. Benkovic, *Trends Biochem. Sci.*, 2017, **42**, 141-154.
5. J. Yin, W. Ren, X. Huang, J. Deng, T. Li and Y. Yin, *Front. Immunol.*, 2018, **9**, 1697.
6. I. T. Sakallioglu, A. S. Maroli, A. De Lima Leite, D. D. Marshall, B. W. Evans, D. K. Zinniel, P. H. Dussault, R. G. Barletta and R. Powers, *J. Am. Chem. Soc.*, 2022, **144**, 21157-21173.
7. M. L. Cheng, Z. M. Bhujwalla and K. Glunde, *Front.Oncol.*, 2016, **6**, 266.
8. J. N. van der Veen, J. P. Kennelly, S. Wan, J. E. Vance, D. E. Vance and R. L. Jacobs, *Biochim.Biophys. Acta Biomembr.*, 2017, **1859**, 1558-1572.
9. J. J. Du, L. Y. Shen, Z. D. Tan, P. W. Zhang, X. Zhao, Y. Xu, M. G. Gan, Q. Yang, J. D. Ma, A. A. Jiang, G. Q. Tang, Y. Z. Jiang, L. Jin, M. Z. Li, L. Bai, X. W. Li, J. Y. Wang, S. H. Zhang and L. Zhu, *Nutrients*, 2018, **10**,131.
10. C. G. Figueroa-Soto and E. M. Valenzuela-Soto, *Biochimie*, 2018, **147**, 89-97.
11. S. S. Li, H. C. Wang, X. X. Wang, Y. Z. Wang and J. Feng, *J. Anim. Sci. Biotechnol.*, 2017, **8**, 72.
12. W. H. Lu, H. H. Chiu, H. C. Kuo, G. Y. Chen, D. Chepyala and C. H. Kuo, *Anal. Chim. Acta.*, 2021, **1149**, 338214.
13. M. Sugimoto, D. T. Wong, A. Hirayama, T. Soga and M. Tomita, *Metabolomics*, 2010, **6**, 78-95.
14. T. S. Wang, P. Španěl and D. Smith, *Int. J. Mass Spectrom*, 2008, **272**, 78-85.
15. L. L. Xu, Y. G. Wang, Z. C. Ma, X. L. Tang and Y. Gao, *Front. Pharmacol.*, 2020, **11**, 1237.
16. X. Y. Si, X. C. Xiong, S. C. Zhang, X. Fang and X. R. Zhang, *Anal. Chem.*, 2017, **89**, 2275-2281.
17. C. Guo, Y. Q. Hu, X. J. Cao and Y. S. *Anal. Chem.*, 2021, **93**, 17060-17068.
18. Y. Chen, H. Chen, G. G. Shi, M. Yang, F. C. Zheng, Z. J. Zheng, S. Y. Zhang and S. L. Zhong, *J.Chromatogr. B.*, 2019, **1128**, 121775.
19. M. Kolisek, R. M. Touyz, A. Romani and M. Barbagallo, *Oxid. Med. Cell. Longevi.*, 2017, **2017**, 7428796.
20. A. Andries, A. Feyaerts, D. Mekahli and A. Van Schepdael, *Electrophoresis*, 2022, **43**, 1010-1018.
21. E. Rackowska, B. Bobrowska-Korczak and J. Giebultowicz, *J. Chromatogr. B*, 2019, **1128**, 121775.
22. M. K. Passarelli, C. F. Newman, P. S. Marshall, A. West, I. S. Gilmore, J. Bunch, M. R. Alexander and C. T. Dollery, *Anal. Chem.*, 2015, **87**, 6696-6702.
23. A. S. Nayak, S. K. Sanganal, S. K. Mudde, A. Oblesha and T. B. Karegoudar, *FEMS Microbiol. Lett.*, 2011, **320**, 128-134.
24. D. Liu, J. P. Huang, S. S. Gao, H. T. Jin and J. M. He, *Acta Pharm. Sin. B*, 2022, **12**, 3341-3353.